

Measurement of the Branching Fraction of and Search for a CP-Violating Asymmetry in $\eta' \rightarrow \pi^+\pi^-e^+e^-$ at BESIII

M. Ablikim¹, M. N. Achasov^{10,c}, P. Adlarson⁶⁴, S. Ahmed¹⁵, M. Albrecht⁴, A. Amoroso^{63A,63C}, Q. An^{60,47}, X. H. Bai⁵⁴, Y. Bai⁴⁶, O. Bakina²⁹, R. Baldini Ferroli^{23A}, I. Balossino^{24A}, Y. Ban^{37,k}, K. Begzsuren²⁶, J. V. Bennett⁵, N. Berger²⁸, M. Bertani^{23A}, D. Bettoni^{24A}, F. Bianchi^{63A,63C}, J. Biernat⁶⁴, J. Bloms⁵⁷, A. Bortone^{63A,63C}, I. Boyko²⁹, R. A. Briere⁵, H. Cai⁶⁵, X. Cai^{1,47}, A. Calcaterra^{23A}, G. F. Cao^{1,51}, N. Cao^{1,51}, S. A. Cetin^{50A}, J. F. Chang^{1,47}, W. L. Chang^{1,51}, G. Chelkov^{29,b}, D. Y. Chen⁶, G. Chen¹, H. S. Chen^{1,51}, M. L. Chen^{1,47}, S. J. Chen³⁵, X. R. Chen²⁵, Y. B. Chen^{1,47}, Z. J. Chen^{20,l}, W. S. Cheng^{63C}, G. Cibinetto^{24A}, F. Cossio^{63C}, X. F. Cui³⁶, H. L. Dai^{1,47}, J. P. Dai^{41,g}, X. C. Dai^{1,51}, A. Dbeyssi¹⁵, R. E. de Boer⁴, D. Dedovich²⁹, Z. Y. Deng¹, A. Denig²⁸, I. Denysenko²⁹, M. Destefanis^{63A,63C}, F. De Mori^{63A,63C}, Y. Ding³³, C. Dong³⁶, J. Dong^{1,47}, L. Y. Dong^{1,51}, M. Y. Dong^{1,47,51}, S. X. Du⁶⁸, J. Fang^{1,47}, S. S. Fang^{1,51}, Y. Fang¹, R. Farinelli^{24A}, L. Fava^{63B,63C}, F. Feldbauer⁴, G. Felici^{23A}, C. Q. Feng^{60,47}, M. Fritsch⁴, C. D. Fu¹, Y. Fu¹, X. L. Gao^{60,47}, Y. Gao⁶¹, Y. Gao^{60,47}, Y. Gao^{37,k}, Y. G. Gao⁶, I. Garzia^{24A,24B}, E. M. Gersabeck⁵⁵, A. Gilman⁵⁶, K. Goetzen¹¹, L. Gong³³, W. X. Gong^{1,47}, W. Gradl²⁸, M. Greco^{63A,63C}, L. M. Gu³⁵, M. H. Gu^{1,47}, S. Gu², Y. T. Gu¹³, C. Y. Guan^{1,51}, A. Q. Guo²², L. B. Guo³⁴, R. P. Guo³⁹, Y. P. Guo^{9,h}, A. Guskov²⁹, S. Han⁶⁵, T. T. Han⁴⁰, T. Z. Han^{9,h}, X. Q. Hao¹⁶, F. A. Harris⁵³, N. Hüskens⁵⁷, K. L. He^{1,51}, F. H. Heinsius⁴, T. Held⁴, Y. K. Heng^{1,47,51}, M. Himmelreich^{11,f}, T. Holtmann⁴, Y. R. Hou⁵¹, Z. L. Hou¹, H. M. Hu^{1,51}, J. F. Hu^{41,g}, T. Hu^{1,47,51}, Y. Hu¹, G. S. Huang^{60,47}, L. Q. Huang⁶¹, X. T. Huang⁴⁰, Y. P. Huang¹, Z. Huang^{37,k}, T. Hussain⁶², W. Ikegami Andersson⁶⁴, W. Imoehl²², M. Irshad^{60,47}, S. Jaeger⁴, S. Janchiv^{26,j}, Q. Ji¹, Q. P. Ji¹⁶, X. B. Ji^{1,51}, X. L. Ji^{1,47}, H. B. Jiang⁴⁰, X. S. Jiang^{1,47,51}, J. B. Jiao⁴⁰, Z. Jiao¹⁸, S. Jin³⁵, Y. Jin⁵⁴, T. Johansson⁶⁴, N. Kalantar-Nayestanaki⁵², X. S. Kang³³, R. Kappert⁵², M. Kavatsyuk⁵², B. C. Ke^{42,1}, I. K. Keshk⁴, A. Khoukaz⁵⁷, P. Kiese²⁸, R. Kiuchi¹, R. Kliemt¹¹, L. Koch³⁰, O. B. Kolcu^{50A,e}, B. Kopf⁴, M. Kuemmel⁴, M. Kuessner⁴, A. Kupsc⁶⁴, M. G. Kurth^{1,51}, W. Kühn³⁰, J. J. Lane⁵⁵, J. S. Lange³⁰, P. Larin¹⁵, A. Lavanian²¹, L. Lavezzi^{63A,63C}, H. Leithoff²⁸, M. Lellmann²⁸, T. Lenz²⁸, C. Li³⁸, C. H. Li³², Cheng Li^{60,47}, D. M. Li⁶⁸, F. Li^{1,47}, G. Li¹, H. Li^{60,47}, H. B. Li^{1,51}, H. J. Li^{9,h}, J. L. Li⁴⁰, J. Q. Li⁴, Ke Li¹, L. K. Li¹, Lei Li³, P. L. Li^{60,47}, P. R. Li³¹, S. Y. Li⁴⁹, W. D. Li^{1,51}, W. G. Li¹, X. H. Li^{60,47}, X. L. Li⁴⁰, Z. Y. Li⁴⁸, H. Liang^{60,47}, H. Liang^{1,51}, Y. F. Liang⁴⁴, Y. T. Liang²⁵, L. Z. Liao^{1,51}, J. Libby²¹, C. X. Lin⁴⁸, B. Liu^{41,g}, B. J. Liu¹, C. X. Liu¹, D. Liu^{60,47}, D. Y. Liu^{41,g}, F. H. Liu⁴³, Fang Liu¹, Feng Liu⁶, H. B. Liu¹³, H. M. Liu^{1,51}, Huanhuan Liu¹, Huihui Liu¹⁷, J. B. Liu^{60,47}, J. Y. Liu^{1,51}, K. Liu¹, K. Y. Liu³³, Ke Liu⁶, L. Liu^{60,47}, Q. Liu⁵¹, S. B. Liu^{60,47}, Shuai Liu⁴⁵, T. Liu^{1,51}, W. M. Liu^{60,47}, X. Liu³¹, Y. B. Liu³⁶, Z. A. Liu^{1,47,51}, Z. Q. Liu⁴⁰, Y. F. Long^{37,k}, X. C. Lou^{1,47,51}, F. X. Lu¹⁶, H. J. Lu¹⁸, J. D. Lu^{1,51}, J. G. Lu^{1,47}, X. L. Lu¹, Y. Lu¹, Y. P. Lu^{1,47}, C. L. Luo³⁴, M. X. Luo⁶⁷, P. W. Luo⁴⁸, T. Luo^{9,h}, X. L. Luo^{1,47}, S. Lusso^{63C}, X. R. Lyu⁵¹, F. C. Ma³³, H. L. Ma¹, L. L. Ma⁴⁰, M. M. Ma^{1,51}, Q. M. Ma¹, R. Q. Ma^{1,51}, R. T. Ma⁵¹, X. N. Ma³⁶, X. X. Ma^{1,51}, X. Y. Ma^{1,47}, Y. M. Ma⁴⁰, F. E. Maas¹⁵, M. Maggiora^{63A,63C}, S. Maldaner⁴, S. Malde⁵⁸, Q. A. Malik⁶², A. Mangoni^{23B}, Y. J. Mao^{37,k}, Z. P. Mao¹, S. Marcello^{63A,63C}, Z. X. Meng⁵⁴, J. G. Messchendorp⁵², G. Mezzadri^{24A}, T. J. Min³⁵, R. E. Mitchell²², X. H. Mo^{1,47,51}, Y. J. Mo⁶, N. Yu. Muchnoi^{10,c}, H. Muramatsu⁵⁶, S. Nakhoul^{11,f}, Y. Nefedov²⁹, F. Nerling^{11,f}, I. B. Nikolaev^{10,c}, Z. Ning^{1,47}, S. Nisar^{8,i}, S. L. Olsen⁵¹, Q. Ouyang^{1,47,51}, S. Pacetti^{23B,23C}, X. Pan^{9,h}, Y. Pan⁵⁵, A. Pathak¹, P. Patteri^{23A}, M. Pelizaeus⁴, H. P. Peng^{60,47}, K. Peters^{11,f}, J. Pettersson⁶⁴, J. L. Ping³⁴, R. G. Ping^{1,51}, A. Pitka⁴, R. Poling⁵⁶, V. Prasad^{60,47}, H. Qi^{60,47}, H. R. Qi⁴⁹, M. Qi³⁵, T. Y. Qi², T. Y. Qi⁹, S. Qian^{1,47}, W. B. Qian⁵¹, Z. Qian⁴⁸, C. F. Qiao⁵¹, L. Q. Qin¹², X. S. Qin⁴, Z. H. Qin^{1,47}, J. F. Qiu¹, S. Q. Qu³⁶, K. H. Rashid⁶², K. Ravindran²¹, C. F. Redmer²⁸, A. Rivetti^{63C}, V. Rodin⁵², M. Rolo^{63C}, G. Rong^{1,51}, Ch. Rosner¹⁵, M. Rump⁵⁷, A. Sarantsev^{29,d}, Y. Schelhaas²⁸, C. Schnier⁴, K. Schoenning⁶⁴, D. C. Shan⁴⁵, W. Shan¹⁹, X. Y. Shan^{60,47}, M. Shao^{60,47}, C. P. Shen⁹, P. X. Shen³⁶, X. Y. Shen^{1,51}, H. C. Shi^{60,47}, R. S. Shi^{1,51}, X. Shi^{1,47}, X. D. Shi^{60,47}, J. J. Song⁴⁰, Q. Q. Song^{60,47}, W. M. Song^{27,1}, Y. X. Song^{37,k}, S. Sosio^{63A,63C}, S. Spataro^{63A,63C}, F. F. Sui⁴⁰, G. X. Sun¹, J. F. Sun¹⁶, L. Sun⁶⁵, S. S. Sun^{1,51}, T. Sun^{1,51}, W. Y. Sun³⁴, X. Sun^{20,l}, Y. J. Sun^{60,47}, Y. K. Sun^{60,47}, Y. Z. Sun¹, Z. T. Sun¹, Y. H. Tan⁶⁵, Y. X. Tan^{60,47}, C. J. Tang⁴⁴, G. Y. Tang¹, J. Tang⁴⁸, J. X. Teng^{60,47}, V. Thoren⁶⁴, I. Uman^{50B}, B. Wang¹, B. L. Wang⁵¹, C. W. Wang³⁵, D. Y. Wang^{37,k}, H. P. Wang^{1,51}, K. Wang^{1,47}, L. L. Wang¹, M. Wang⁴⁰, M. Z. Wang^{37,k}, Meng Wang^{1,51}, W. H. Wang⁶⁵, W. P. Wang^{60,47}, X. Wang^{37,k}, X. F. Wang³¹, X. L. Wang^{9,h}, Y. Wang⁴⁸, Y. Wang^{60,47}, Y. D. Wang¹⁵, Y. F. Wang^{1,47,51}, Y. Q. Wang¹, Z. Wang^{1,47}, Z. Y. Wang¹, Ziyi Wang⁵¹, Zongyuan Wang^{1,51}, D. H. Wei¹², P. Weidenkaff²⁸, F. Weidner⁵⁷, S. P. Wen¹, D. J. White⁵⁵, U. Wiedner⁴, G. Wilkinson⁵⁸, M. Wolke⁶⁴, L. Wollenberg⁴, J. F. Wu^{1,51}, L. H. Wu¹, L. J. Wu^{1,51}, X. Wu^{9,h}, Z. Wu^{1,47}, L. Xia^{60,47}, H. Xiao^{9,h}, S. Y. Xiao¹, Y. J. Xiao^{1,51}, Z. J. Xiao³⁴, X. H. Xie^{37,k}, Y. G. Xie^{1,47}, Y. H. Xie⁶, T. Y. Xing^{1,51}, X. A. Xiong^{1,51}, G. F. Xu¹, J. J. Xu³⁵, Q. J. Xu¹⁴, W. Xu^{1,51}, X. P. Xu⁴⁵, Y. C. Xu⁵¹, F. Yan^{9,h}, L. Yan^{63A,63C}, L. Yan^{9,h}, W. B. Yan^{60,47}, W. C. Yan⁶⁸, Xu Yan⁴⁵, H. J. Yang^{41,g}, H. X. Yang¹, L. Yang⁶⁵, R. X. Yang^{60,47}, S. L. Yang^{1,51}, Y. H. Yang³⁵, Y. X. Yang¹², Yifan Yang^{1,51}, Zhi Yang²⁵, M. Ye^{1,47}, M. H. Ye⁷, J. H. Yin¹, Z. Y. You⁴⁸, B. X. Yu^{1,47,51}, C. X. Yu³⁶, G. Yu^{1,51}, J. S. Yu^{20,l}, T. Yu⁶¹, C. Z. Yuan^{1,51}, W. Yuan^{63A,63C}, X. Q. Yuan^{37,k}, Y. Yuan¹, Z. Y. Yuan⁴⁸, C. X. Yue³², A. Yuncu^{50A,a}, A. A. Zafar⁶², Y. Zeng^{20,l}, B. X. Zhang¹, Guangyi Zhang¹⁶, H. Zhang⁶⁰, H. H. Zhang⁴⁸, H. Y. Zhang^{1,47}, J. L. Zhang⁶⁶, J. Q. Zhang³⁴, J. Q. Zhang⁴, J. W. Zhang^{1,47,51}, J. Y. Zhang¹, J. Z. Zhang^{1,51}, Jianyu Zhang^{1,51}, Jiawei Zhang^{1,51}, Lei Zhang³⁵, S. Zhang⁴⁸, S. F. Zhang³⁵, T. J. Zhang^{41,g}, X. Y. Zhang⁴⁰, Y. Zhang⁵⁸, Y. H. Zhang^{1,47}, Y. T. Zhang^{60,47}, Yan Zhang^{60,47}, Yao Zhang¹, Yi Zhang^{9,h}, Z. H. Zhang⁶, Z. Y. Zhang⁶⁵, G. Zhao¹, J. Zhao³², J. Y. Zhao^{1,51}, J. Z. Zhao^{1,47}, Lei Zhao^{60,47}, Ling Zhao¹, M. G. Zhao³⁶, Q. Zhao¹, S. J. Zhao⁶⁸, Y. B. Zhao^{1,47}, Y. X. Zhao²⁵, Z. G. Zhao^{60,47}, A. Zhemchugov^{29,b}, B. Zheng⁶¹, J. P. Zheng^{1,47}, Y. Zheng^{37,k}, Y. H. Zheng⁵¹, B. Zhong³⁴, C. Zhong⁶¹, L. P. Zhou^{1,51}, Q. Zhou^{1,51}, X. Zhou⁶⁵, X. K. Zhou⁵¹, X. R. Zhou^{60,47}, A. N. Zhu^{1,51}, J. Zhu³⁶, K. Zhu¹, K. J. Zhu^{1,47,51}, S. H. Zhu⁵⁹, W. J. Zhu³⁶, Y. C. Zhu^{60,47}, Z. A. Zhu^{1,51}, B. S. Zou¹, J. H. Zou¹

(BESIII Collaboration)

- ¹ Institute of High Energy Physics, Beijing 100049, People's Republic of China
- ² Beihang University, Beijing 100191, People's Republic of China
- ³ Beijing Institute of Petrochemical Technology, Beijing 102617, People's Republic of China
- ⁴ Bochum Ruhr-University, D-44780 Bochum, Germany
- ⁵ Carnegie Mellon University, Pittsburgh, Pennsylvania 15213, USA
- ⁶ Central China Normal University, Wuhan 430079, People's Republic of China
- ⁷ China Center of Advanced Science and Technology, Beijing 100190, People's Republic of China
- ⁸ COMSATS University Islamabad, Lahore Campus, Defence Road, Off Raiwind Road, 54000 Lahore, Pakistan
- ⁹ Fudan University, Shanghai 200443, People's Republic of China
- ¹⁰ G.I. Budker Institute of Nuclear Physics SB RAS (BINP), Novosibirsk 630090, Russia
- ¹¹ GSI Helmholtzcentre for Heavy Ion Research GmbH, D-64291 Darmstadt, Germany
- ¹² Guangxi Normal University, Guilin 541004, People's Republic of China
- ¹³ Guangxi University, Nanning 530004, People's Republic of China
- ¹⁴ Hangzhou Normal University, Hangzhou 310036, People's Republic of China
- ¹⁵ Helmholtz Institute Mainz, Johann-Joachim-Becher-Weg 45, D-55099 Mainz, Germany
- ¹⁶ Henan Normal University, Xinxiang 453007, People's Republic of China
- ¹⁷ Henan University of Science and Technology, Luoyang 471003, People's Republic of China
- ¹⁸ Huangshan College, Huangshan 245000, People's Republic of China
- ¹⁹ Hunan Normal University, Changsha 410081, People's Republic of China
- ²⁰ Hunan University, Changsha 410082, People's Republic of China
- ²¹ Indian Institute of Technology Madras, Chennai 600036, India
- ²² Indiana University, Bloomington, Indiana 47405, USA
- ²³ INFN Laboratori Nazionali di Frascati, (A)INFN Laboratori Nazionali di Frascati, I-00044, Frascati, Italy; (B)INFN Sezione di Perugia, I-06100, Perugia, Italy; (C)University of Perugia, I-06100, Perugia, Italy
- ²⁴ INFN Sezione di Ferrara, (A)INFN Sezione di Ferrara, I-44122, Ferrara, Italy; (B)University of Ferrara, I-44122, Ferrara, Italy
- ²⁵ Institute of Modern Physics, Lanzhou 730000, People's Republic of China
- ²⁶ Institute of Physics and Technology, Peace Ave. 54B, Ulaanbaatar 13330, Mongolia
- ²⁷ Jilin University, Changchun 130012, People's Republic of China
- ²⁸ Johannes Gutenberg University of Mainz, Johann-Joachim-Becher-Weg 45, D-55099 Mainz, Germany
- ²⁹ Joint Institute for Nuclear Research, 141980 Dubna, Moscow region, Russia
- ³⁰ Justus-Liebig-Universität Giessen, II. Physikalisches Institut, Heinrich-Buff-Ring 16, D-35392 Giessen, Germany
- ³¹ Lanzhou University, Lanzhou 730000, People's Republic of China
- ³² Liaoning Normal University, Dalian 116029, People's Republic of China
- ³³ Liaoning University, Shenyang 110036, People's Republic of China
- ³⁴ Nanjing Normal University, Nanjing 210023, People's Republic of China
- ³⁵ Nanjing University, Nanjing 210093, People's Republic of China
- ³⁶ Nankai University, Tianjin 300071, People's Republic of China
- ³⁷ Peking University, Beijing 100871, People's Republic of China
- ³⁸ Qufu Normal University, Qufu 273165, People's Republic of China
- ³⁹ Shandong Normal University, Jinan 250014, People's Republic of China
- ⁴⁰ Shandong University, Jinan 250100, People's Republic of China
- ⁴¹ Shanghai Jiao Tong University, Shanghai 200240, People's Republic of China
- ⁴² Shanxi Normal University, Linfen 041004, People's Republic of China
- ⁴³ Shanxi University, Taiyuan 030006, People's Republic of China
- ⁴⁴ Sichuan University, Chengdu 610064, People's Republic of China
- ⁴⁵ Soochow University, Suzhou 215006, People's Republic of China
- ⁴⁶ Southeast University, Nanjing 211100, People's Republic of China
- ⁴⁷ State Key Laboratory of Particle Detection and Electronics, Beijing 100049, Hefei 230026, People's Republic of China
- ⁴⁸ Sun Yat-Sen University, Guangzhou 510275, People's Republic of China
- ⁴⁹ Tsinghua University, Beijing 100084, People's Republic of China
- ⁵⁰ Turkish Accelerator Center Particle Factory Group, (A)Istanbul Bilgi University, 34060 Eyup, Istanbul, Turkey; (B)Near East University, Nicosia, North Cyprus, Mersin 10, Turkey
- ⁵¹ University of Chinese Academy of Sciences, Beijing 100049, People's Republic of China
- ⁵² University of Groningen, NL-9747 AA Groningen, The Netherlands
- ⁵³ University of Hawaii, Honolulu, Hawaii 96822, USA
- ⁵⁴ University of Jinan, Jinan 250022, People's Republic of China
- ⁵⁵ University of Manchester, Oxford Road, Manchester, M13 9PL, United Kingdom
- ⁵⁶ University of Minnesota, Minneapolis, Minnesota 55455, USA
- ⁵⁷ University of Muenster, Wilhelm-Klemm-Str. 9, 48149 Muenster, Germany
- ⁵⁸ University of Oxford, Keble Rd, Oxford, UK OX13RH
- ⁵⁹ University of Science and Technology Liaoning, Anshan 114051, People's Republic of China
- ⁶⁰ University of Science and Technology of China, Hefei 230026, People's Republic of China
- ⁶¹ University of South China, Hengyang 421001, People's Republic of China

⁶² University of the Punjab, Lahore-54590, Pakistan

⁶³ University of Turin and INFN, (A)University of Turin, I-10125, Turin, Italy; (B)University of Eastern Piedmont, I-15121, Alessandria, Italy; (C)INFN, I-10125, Turin, Italy

⁶⁴ Uppsala University, Box 516, SE-75120 Uppsala, Sweden

⁶⁵ Wuhan University, Wuhan 430072, People's Republic of China

⁶⁶ Xinyang Normal University, Xinyang 464000, People's Republic of China

⁶⁷ Zhejiang University, Hangzhou 310027, People's Republic of China

⁶⁸ Zhengzhou University, Zhengzhou 450001, People's Republic of China

^a Also at Bogazici University, 34342 Istanbul, Turkey

^b Also at the Moscow Institute of Physics and Technology, Moscow 141700, Russia

^c Also at the Novosibirsk State University, Novosibirsk, 630090, Russia

^d Also at the NRC "Kurchatov Institute", PNPI, 188300, Gatchina, Russia

^e Also at Istanbul Arel University, 34295 Istanbul, Turkey

^f Also at Goethe University Frankfurt, 60323 Frankfurt am Main, Germany

^g Also at Key Laboratory for Particle Physics, Astrophysics and Cosmology, Ministry of Education; Shanghai Key Laboratory for Particle Physics and Cosmology; Institute of Nuclear and Particle Physics, Shanghai 200240, People's Republic of China

^h Also at Key Laboratory of Nuclear Physics and Ion-beam Application (MOE) and Institute of Modern Physics, Fudan University, Shanghai 200443, People's Republic of China

ⁱ Also at Harvard University, Department of Physics, Cambridge, MA, 02138, USA

^j Currently at: Institute of Physics and Technology, Peace Ave.54B, Ulaanbaatar 13330, Mongolia

^k Also at State Key Laboratory of Nuclear Physics and Technology,

Peking University, Beijing 100871, People's Republic of China

^l School of Physics and Electronics, Hunan University, Changsha 410082, China

(Dated: April 29, 2021)

The rare decay $\eta' \rightarrow \pi^+\pi^-e^+e^-$ is studied using a sample of 1.3×10^9 J/ψ events collected with the BESIII detector at BEPCII in 2009 and 2012. The branching fraction is measured with improved precision to be $(2.42 \pm 0.05_{\text{stat.}} \pm 0.08_{\text{syst.}}) \times 10^{-3}$. Due to the inclusion of new data, this result supersedes the last BESIII result on this branching fraction. In addition, the CP-violating asymmetry in the angle between the decay planes of the $\pi^+\pi^-$ -pair and the e^+e^- -pair is investigated. A measurable value would indicate physics beyond the standard model; the result is $\mathcal{A}_{CP} = (2.9 \pm 3.7_{\text{stat.}} \pm 1.1_{\text{syst.}})\%$, which is consistent with the standard model expectation of no CP-violation. The precision is comparable to the asymmetry measurement in the $K_L^0 \rightarrow \pi^+\pi^-e^+e^-$ decay where the observed $(14 \pm 2)\%$ effect is driven by a standard model mechanism.

PACS numbers: 13.25.Gv, 12.38.Qk, 14.20.Gk, 14.40.Cs

I. INTRODUCTION

At the precision/intensity frontier of particle physics, rare decays of light mesons such as the η' are valuable laboratories for the study of a number of interesting phenomena. They offer a way of testing the effective field theories that describe quantum chromodynamics at low energies. In addition, they provide an excellent window for physics beyond the standard model (SM), since small SM rates make possible new contributions easier to detect.

The decay $\eta' \rightarrow \pi^+\pi^-\gamma^* \rightarrow \pi^+\pi^-e^+e^-$, can be described both by vector meson dominance (VMD) models [1, 2] and by unitary chiral perturbation theory [3]. Precise experimental data is needed to guide phenomenological descriptions of the reaction. The process $\eta' \rightarrow \pi^+\pi^-e^+e^-$ is expected to proceed through an intermediate virtual photon, with dynamics closely related to the decay $\eta' \rightarrow \pi^+\pi^-\gamma$ which has been studied recently by the BESIII experiment [4]. As in the $\eta' \rightarrow \pi^+\pi^-\gamma$ decay, $\eta' \rightarrow \pi^+\pi^-e^+e^-$ is expected to exhibit a contribution from the box anomaly of the Wess-Zumino-Witten La-

grangian [5] and a dominant $\rho \rightarrow \pi^+\pi^-$ contribution.

A new aspect of $\eta' \rightarrow \pi^+\pi^-e^+e^-$ compared to $\eta' \rightarrow \pi^+\pi^-\gamma$ is that in analogy with the decay $K_L^0 \rightarrow \pi^+\pi^-\gamma^* \rightarrow \pi^+\pi^-e^+e^-$ studied in Refs. [6, 7], it allows for a test of CP-violation due to the interference between the dominating, CP-conserving, magnetic transition, and a possible CP-violating electric dipole type transition [8–10]. Such an interference term is proportional to $\sin 2\varphi$, where φ is the angle between the decay planes of the e^+e^- -pair and the $\pi^+\pi^-$ -pair in the reference frame of the η' -meson as shown in Fig. 1 and unambiguously defined by Eqs 4 to 8. Hence, an electric dipole transition will manifest itself as an asymmetry \mathcal{A}_{CP} of the $\sin 2\varphi$ distribution [2, 9]

$$\begin{aligned} \mathcal{A}_{CP} &= \langle \text{sgn}(\sin 2\varphi) \rangle \\ &= \frac{1}{\Gamma} \int_0^{2\pi} \frac{d\Gamma}{d\varphi} \text{sgn}(\sin 2\varphi) d\varphi, \end{aligned} \quad (1)$$

where Γ is the total decay width, sgn is the sign function, and $d\Gamma/d\varphi$ is the partial decay width for $\eta' \rightarrow \pi^+\pi^-e^+e^-$. Experimentally, this quantity can be ex-

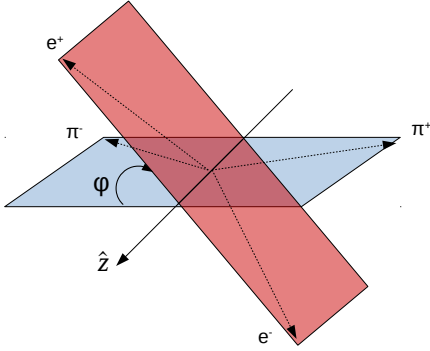


FIG. 1: Illustration of the decay plane angle φ . \hat{z} is a unit vector along the intersection of the two decay planes. φ can be unambiguously determined from Eqs. 4 to 8.

tracted as:

$$\mathcal{A}_\varphi = \frac{N(\sin 2\varphi > 0) - N(\sin 2\varphi < 0)}{N(\sin 2\varphi > 0) + N(\sin 2\varphi < 0)}, \quad (2)$$

where $N(x)$ is the acceptance-corrected number of events in the corresponding angular region.

The first experimental evidence of the decay $\eta' \rightarrow \pi^+\pi^-e^+e^-$ was obtained by the CLEO experiment [11]. The branching fraction was determined to be $(2.5^{+1.2}_{-0.9} \pm 0.5) \times 10^{-3}$ from $7.9^{+3.9}_{-2.7}$ events. The most precise measurement of the branching fraction to date was made by the BESIII experiment using 225 million J/ψ events collected in 2009 [12]. The branching fraction was determined to be $(2.11 \pm 0.12(\text{stat.}) \pm 0.15(\text{syst.})) \times 10^{-3}$ from 429 ± 24 events.

The asymmetry \mathcal{A}_φ has been measured for the decay $\eta \rightarrow \pi^+\pi^-e^+e^-$ by the WASA-at-COSY [13] and KLOE [14] experiments, and was found to be consistent with zero in both cases. The asymmetry has never been measured in the decay $\eta' \rightarrow \pi^+\pi^-e^+e^-$. This work aims to reduce the statistical uncertainty on the branching fraction by the inclusion of an additional 1.085 billion J/ψ events collected by the BESIII experiment in 2012 [15, 16] and perform the first measurement of the asymmetry \mathcal{A}_φ .

II. DETECTOR AND DATA SAMPLES

In this work, 1.31×10^9 J/ψ meson decays [15, 16] collected by BESIII in 2009 and 2012 are analyzed. Through the radiative decay $J/\psi \rightarrow \gamma\eta'$, this yields a sample of about 6.7 million η' events.

The BESIII detector is a magnetic spectrometer [17] collecting data at the Beijing Electron Positron Collider II (BEPCII) [18]. It covers 93% of the solid angle, and consists of a helium-based multilayer drift

chamber (MDC), a plastic scintillator time-of-flight system (TOF), and a CsI(Tl) electromagnetic calorimeter (EMC), which are all enclosed in a superconducting solenoidal magnet providing a 1.0 T (0.9 T in 2012) magnetic field. The solenoid is supported by an octagonal flux-return yoke with resistive plate counter muon identifier modules interleaved with steel. The charged-particle momentum resolution at 1 GeV/c is 0.5%, and the dE/dx resolution is 6% for the electrons from Bhabha scattering. The EMC measures photon energies with a resolution of 2.5% (5%) at 1 GeV in the barrel (end cap) region. The time resolution of the TOF barrel part is 68 ps, while that of the end cap part is 110 ps.

For determination of detection efficiencies and estimation of background, Monte Carlo (MC) samples are produced with a GEANT4-based [19] detector simulation package BOOST [20], which includes the geometry and response of the BESIII detector. The beam energy spread and initial state radiation (ISR) in the e^+e^- annihilations is modelled with the generator KKMC [21]. For qualitative studies of the background contributions, an inclusive MC sample is used. For this sample, the J/ψ resonance as well as continuum processes are produced by KKMC [21]. Known decay modes are modelled with EVTGEN [22, 23] using branching fractions taken from the Particle Data Group (PDG) [24], and the remaining unknown decays from the charmonium states are produced with LUNDCHARM [25]. Final state radiation (FSR) from charged particles is incorporated with the PHOTOS package [26]. The decay $J/\psi \rightarrow \gamma\eta'$ is generated with the HELAMP model of EVTGEN [27]. Specific generators based on EVTGEN have been developed for the decays $\eta' \rightarrow \pi^+\pi^-e^+e^-$ [28] and $\eta' \rightarrow \pi^+\pi^-\gamma$ [4] using theoretical decay amplitudes from the VMD model [2]. The MC samples referred to as *signal MC* throughout the text have been generated using the former generator.

III. ANALYSIS

In order to minimize the impact of systematic effects due to the number of J/ψ mesons, tracking and charged particle identification (PID) of pions, as well as the reconstruction of photons, the branching fraction of $\eta' \rightarrow \pi^+\pi^-e^+e^-$ is determined relative to the channel $\eta' \rightarrow \pi^+\pi^-\gamma$. This is the second most probable decay of the η' meson, and its branching fraction is well known [4, 24, 29]. The branching fraction for $\eta' \rightarrow \pi^+\pi^-e^+e^-$ is calculated according to

$$\mathcal{B}(\eta' \rightarrow \pi^+\pi^-e^+e^-) = \frac{N_{\eta' \rightarrow \pi^+\pi^-e^+e^-} \times \varepsilon_{\eta' \rightarrow \pi^+\pi^-\gamma} \times \mathcal{B}(\eta' \rightarrow \pi^+\pi^-\gamma)}{N_{\eta' \rightarrow \pi^+\pi^-\gamma} \times \varepsilon_{\eta' \rightarrow \pi^+\pi^-e^+e^-}}, \quad (3)$$

where N_i is the event yield in channel i , ε_i is the corresponding efficiency, and $\mathcal{B}(\eta' \rightarrow \pi^+\pi^-\gamma)$ is the branching fraction for the decay $\eta' \rightarrow \pi^+\pi^-\gamma$.

A. Signal: $\eta' \rightarrow \pi^+\pi^-e^+e^-$

The signal channel is studied through the decay chain $J/\psi \rightarrow \gamma\eta'$, $\eta' \rightarrow \pi^+\pi^-e^+e^-$. Each event is required to contain four charged track candidates with net charge zero, and at least one photon candidate. The MDC enables reconstruction of charged tracks within $|\cos\theta| < 0.93$, where θ is the polar angle of the track relative to the symmetry axis of the detector. Tracks are also required to originate from a region within 10 cm of the interaction point (IP) in the longitudinal direction, and 1 cm in the transverse direction.

Photons are reconstructed from showers with a deposited energy of at least 25 MeV in the barrel EMC ($|\cos\theta| < 0.80$), or at least 50 MeV in the endcap EMC ($0.86 < |\cos\theta| < 0.92$). To ensure that these showers originate from a photon, the angle between the shower and the nearest charged track is required to be larger than 15° . Finally, photons are required to arrive within 700 ns from the event start time in order to reduce background from photons that do not originate from the same event.

For each candidate event, TOF and dE/dx information is used to perform PID. Furthermore, a four-constraint (4C) kinematic fit of all final state particles to the initial J/ψ four momentum is performed. For both the PID and kinematic fit, the hypotheses $\gamma\pi^+\pi^-e^+e^-$, $\gamma\pi^+\pi^-\mu^+\mu^-$ and $\gamma\pi^+\pi^-\pi^+\pi^-$ are tested. The hypotheses are evaluated with the combined $\chi^2_{4C+PID} = \chi^2_{4C} + \sum_{j=1}^4 \chi^2_{PID}(j)$, where $\chi^2_{PID}(j)$ is the PID χ^2 for track j . Only those events where the $\gamma\pi^+\pi^-e^+e^-$ hypothesis is best are kept. If the event contains more than one candidate photon, the one that gives the least χ^2_{4C} is selected. Finally, an upper limit on $\chi^2_{4C+PID} < 62$ is imposed. This cut-off has been optimized with respect to the figure of merit $N_S/\sqrt{N_D}$, where N_S is the number of events in the signal MC sample, and N_D is the number of events in data after the final selection.

After this preselection, an η' peak is clearly visible in the invariant mass spectrum of $\pi^+\pi^-e^+e^-$ as shown in Fig. 2 (a). However, studies of an inclusive MC sample of $1.2 \times 10^9 J/\psi$ events show that there is significant background from $\eta' \rightarrow \pi^+\pi^-\gamma$ events, where the photon converts to an e^+e^- -pair in the beam pipe or the inner wall of the drift chamber. One would expect the invariant mass of such conversion pairs to be close to zero. However, the BESIII tracking algorithm uses the origin as a reference point for all tracks. This means that the direction of tracks that originate elsewhere will be mis-reconstructed. Hence, conversion pairs gain an artificial opening angle, and their reconstructed invariant masses are larger than the true values. Therefore, the conversion background appears as the large peak at about 0.015 GeV/c^2 in the e^+e^- invariant mass distribution in Fig. 2 (b). By finding the intersection of the e^+ - and e^- -helices in the $r-\phi$ projection, one acquires a measure of the distance from the e^+e^- -vertex position to the IP, R_{xy} . Figure 3 shows

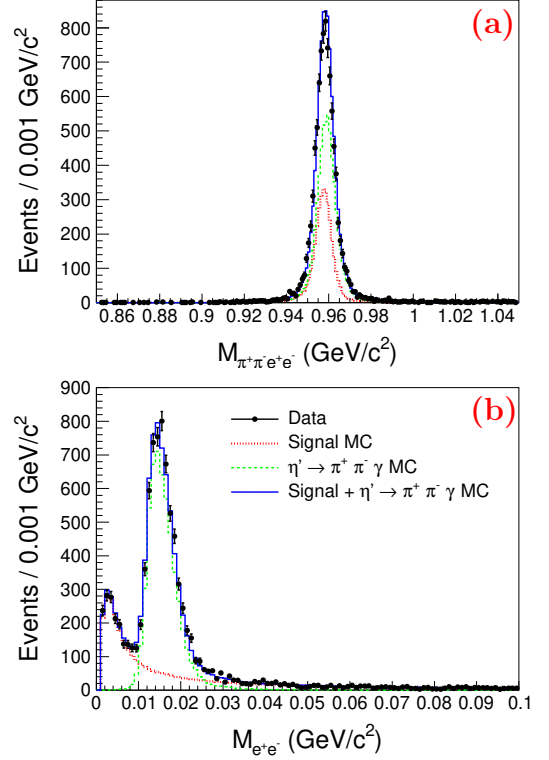


FIG. 2: Invariant mass distributions of $\pi^+\pi^-e^+e^-$ (a) and e^+e^- (b) for events after the preselection. The dots with error bars correspond to data, the dotted (red) histogram represents the signal MC sample, the dashed (green) histogram represents the $\eta' \rightarrow \pi^+\pi^-\gamma$ MC sample, and the solid (blue) histogram is the sum of the two contributions. The two contributions are normalized according to their respective branching fractions and their efficiencies as determined from the MC simulation.

R_{xy} for the selected events. From this distribution, it is clear that the e^+e^- -pairs are created at three characteristic locations in the detector. The signal pairs effectively originate from the IP, whereas the conversion background pairs come from two different regions: at $R_{xy} \approx 3$ cm, corresponding to the beam pipe, and at $R_{xy} \approx 6$ cm, corresponding to the inner wall of the MDC. In order to reject photon conversion events and improve the signal-to-background ratio, two additional discriminating variables are introduced. The first one, the invariant mass of the e^+e^- -pair at the beam pipe, M_{ee}^{BP} , is determined by changing the reference point of the helices of all e^\pm tracks to their respective points of intersection with the beam pipe, and subsequently recalculating the momentum vectors. This procedure changes the direction of the vectors, but not their magnitudes. For e^+e^- pairs that originate from the IP, the opening angle is increased, and as a consequence, their invariant masses become larger than the true value. The momenta of the e^+e^- pairs that were created in the beam pipe will instead be approximately parallel and the invariant mass close to the minimum value, $2m_e$. The second variable is the z -projection of

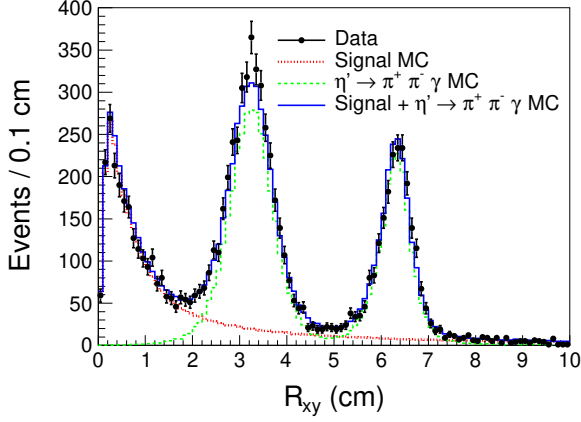


FIG. 3: Distribution of the distance of the e^+e^- -vertex from the IP in the transverse direction. The dots with error bars correspond to data, the dotted (red) histogram represents the signal MC sample, the dashed (green) histogram represents the $\eta' \rightarrow \pi^+\pi^-\gamma$ MC sample, and the solid (blue) histogram is the sum of the two contributions. The two contributions are normalized according to their respective branching fractions and their efficiencies as determined from the MC simulation.

the opening angle of the e^+e^- -pair, where z is the magnetic field direction, Φ_{ee} [30]. In conversion events, Φ_{ee} is expected to be close to zero, whereas in η' decays it varies widely. In the two-dimensional distributions of M_{ee}^{BP} vs. R_{xy} , and Φ_{ee} vs. R_{xy} , shown in Fig. 4, signal events and photon conversion events are well separated. By selecting appropriate regions of these distributions, the photon conversion events can be vetoed. First, we require $\Phi_{ee} < 75^\circ$ when $1.8 \text{ cm} < R_{xy} < 7.5 \text{ cm}$. Then, in the M_{ee}^{BP} vs. R_{xy} distribution, we select all events to the high mass side of a curve defined by straight line segments between the points $(0.004 \text{ GeV}/c^2, 0 \text{ cm})$, $(0.004 \text{ GeV}/c^2, 2 \text{ cm})$, $(0.03 \text{ GeV}/c^2, 3 \text{ cm})$, and $(0.07 \text{ GeV}/c^2, 10 \text{ cm})$.

After the application of the photon conversion veto, most conversion events have been rejected, and the $\pi^+\pi^-e^+e^-$ mass peak is very clean, as shown in Fig. 5. Furthermore data and signal MC simulations are in good agreement in both the e^+e^- and $\pi^+\pi^-$ invariant mass distributions. Finally, we define the signal region as $|M_{\pi^+\pi^-e^+e^-} - m_{\eta'}| < 0.02 \text{ GeV}/c^2$, where $m_{\eta'}$ is the mass of the η' given by the PDG [24]. The signal purity of the sample is estimated to be 98% based on our MC simulations of $\eta' \rightarrow \pi^+\pi^-\gamma$. Accordingly, a residual contribution of 48 $\eta' \rightarrow \pi^+\pi^-\gamma$ events is subtracted. The number of combinatorial background events remaining is estimated from the η' -sidebands in the $M_{\pi^+\pi^-e^+e^-}$ distribution, defined as $0.06 \text{ GeV}/c^2 < |M_{\pi^+\pi^-e^+e^-} - m_{\eta'}| < 0.08 \text{ GeV}/c^2$. The number of events remaining after these subtractions is taken as the final yield for $\eta' \rightarrow \pi^+\pi^-e^+e^-$ and is listed in Table I together with the detection efficiency.

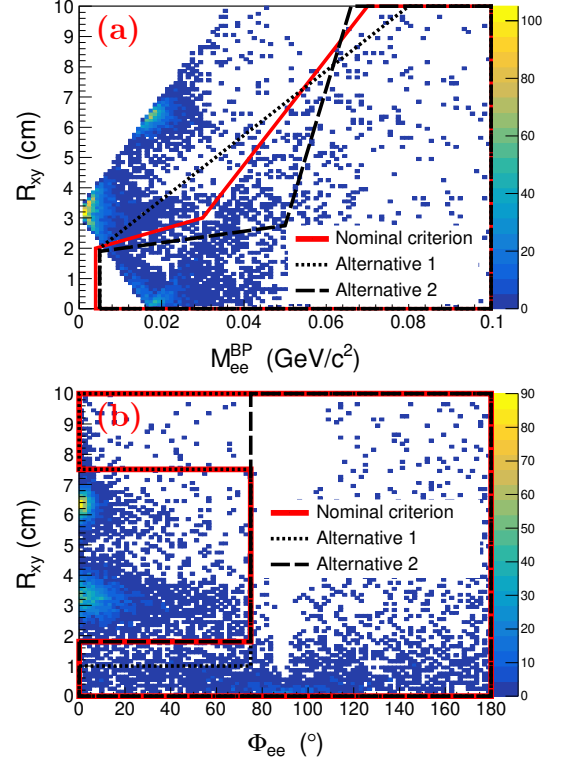


FIG. 4: Photon conversion veto criterion on the M_{ee}^{BP} vs. R_{xy} (a) and Φ_{ee} vs. R_{xy} (b) plots from data. All events outside the solid (red) polygons are rejected. The dashed and dotted lines in each plot show the two alternative areas used to evaluate the systematic uncertainty due to the photon conversion veto.

TABLE I: Efficiencies and event yields for the signal and normalization channels

Channel	$\varepsilon[\%]$	Yield
$\eta' \rightarrow \pi^+\pi^-e^+e^-$	15.25 ± 0.01	2584 ± 52
$\eta' \rightarrow \pi^+\pi^-\gamma$	38.09 ± 0.01	786200 ± 900

The quantity $\sin 2\varphi$ is calculated for each event using the method described in Ref. [14]. The orientation of the decay planes is given by the unit normal vectors defined as:

$$\hat{n}_e = \frac{\mathbf{p}_{e^+} \times \mathbf{p}_{e^-}}{|\mathbf{p}_{e^+} \times \mathbf{p}_{e^-}|} \text{ and } \hat{n}_\pi = \frac{\mathbf{p}_{\pi^+} \times \mathbf{p}_{\pi^-}}{|\mathbf{p}_{\pi^+} \times \mathbf{p}_{\pi^-}|}, \quad (4)$$

where \mathbf{p}_{π^\pm} , \mathbf{p}_{e^\pm} are the momenta of the pions and electrons in the η' rest frame, respectively. It follows from the properties of the dot product that:

$$\hat{n}_e \cdot \hat{n}_\pi = \cos \varphi \text{ and } |\hat{n}_e \times \hat{n}_\pi| = |\sin \varphi|, \quad (5)$$

where φ is the angle between the normal vectors, i.e., the asymmetry angle. The sign of $\sin \varphi$ is obtained by using the direction of the unit vector along the intersection of

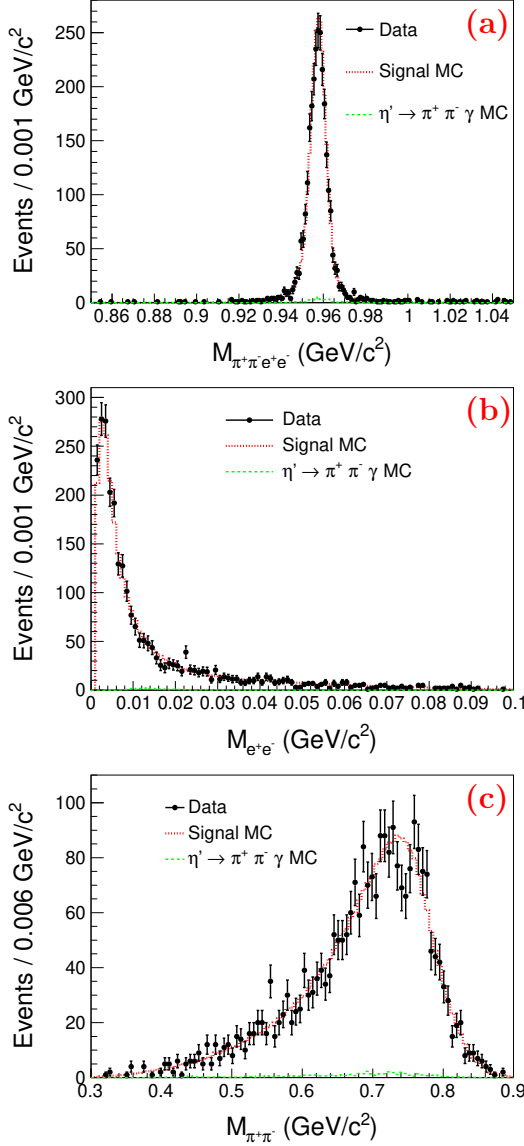


FIG. 5: Invariant mass distributions of $\pi^+\pi^-e^+e^-$ (a), e^+e^- (b) and $\pi^+\pi^-$ (c) for events after the photon conversion veto. Dots with error bars represent data, the dotted (red) histogram represents the signal MC sample, and the dashed (green) histogram the remaining background contribution from $\eta' \rightarrow \pi^+\pi^-\gamma$ events.

the two planes (see Fig. 1)

$$\hat{z} = \frac{\mathbf{p}_{e^+} + \mathbf{p}_{e^-}}{|\mathbf{p}_{e^+} + \mathbf{p}_{e^-}|} \quad (6)$$

and then $\sin \varphi$ is calculated as

$$\sin \varphi = (\hat{n}_e \times \hat{n}_\pi) \cdot \hat{z}. \quad (7)$$

The final expression for $\sin 2\varphi$ is

$$\sin 2\varphi = 2 \sin \varphi \cos \varphi = 2 [(\hat{n}_e \times \hat{n}_\pi) \cdot \hat{z}] (\hat{n}_e \cdot \hat{n}_\pi). \quad (8)$$

The $\sin 2\varphi$ distributions from data and the $\eta' \rightarrow \pi^+\pi^-e^+e^-$ MC sample are shown in Fig. 7. The sig-

TABLE II: Efficiencies and event yields in the two regions of the decay plane angle φ .

Region	$\varepsilon[\%]$	Yield
$\sin 2\varphi > 0$	15.95 ± 0.02	1331 ± 40
$\sin 2\varphi < 0$	15.93 ± 0.02	1287 ± 37

nal yields for events with $\sin 2\varphi > 0$ and $\sin 2\varphi < 0$ are determined by fits to the two $\pi^+\pi^-e^+e^-$ invariant mass distributions. The fits are performed in the range $0.91 \text{ GeV}/c^2 < M_{\pi^+\pi^-e^+e^-} < 1.00 \text{ GeV}/c^2$, where the signal is represented by the MC lineshape convolved with a Gaussian function to account for differences in detector resolution between data and MC simulations. Combinatorial background is represented by a second order Chebychev polynomial. Peaking backgrounds are subtracted based on MC simulations.

Limited momentum resolution will cause some fraction α of events with a true value $\sin 2\varphi < 0$ to be reconstructed with a value $\sin 2\varphi > 0$ and vice versa. This migration effect must be corrected for in order to obtain an unbiased estimate of the asymmetry of the sample. By studying our signal MC sample, we find that the fraction of events that migrate from $\sin 2\varphi > 0$ to $\sin 2\varphi < 0$ is the same as that which migrates from $\sin 2\varphi < 0$ to $\sin 2\varphi > 0$, and we estimate it to be $21.3 \pm 0.1\%$. Given that the efficiencies in the two regions are the same within the uncertainty, see Table II, the asymmetry corrected for bin migration in $\sin 2\varphi$ is

$$\mathcal{A}_{\varphi, \text{corr.}} = \frac{\mathcal{A}_{\varphi, \text{rec.}}}{1 - 2\alpha}, \quad (9)$$

where $\mathcal{A}_{\varphi, \text{rec.}}$ is the asymmetry acquired by inserting the event yields into Eq. 2.

The accuracy of the method used to estimate the asymmetry is evaluated by applying it to nine MC ensembles generated with asymmetries ranging from -20% to $+20\%$ in steps of 5% . In each ensemble there are 125 samples, and each sample matches our data in size. The asymmetry is extracted from each sample and compared to the expected value as is shown in Fig. 6. It is clear that, on average, the true value of the asymmetry can be reliably reproduced.

B. Normalization Channel: $\eta' \rightarrow \pi^+\pi^-\gamma$

To select the decay $\eta' \rightarrow \pi^+\pi^-\gamma$, at least two photons and exactly two charged tracks with zero net charge are required. The radiative photon coming from the initial J/ψ decay is monoenergetic at $E_{\gamma_{\text{rad}}} = 1.4 \text{ GeV}$ and we require one photon to have an energy in a 20 MeV window around that value. In all other aspects, the event selection procedure for this channel is identical to that described in the previous section. The optimal cutoff for

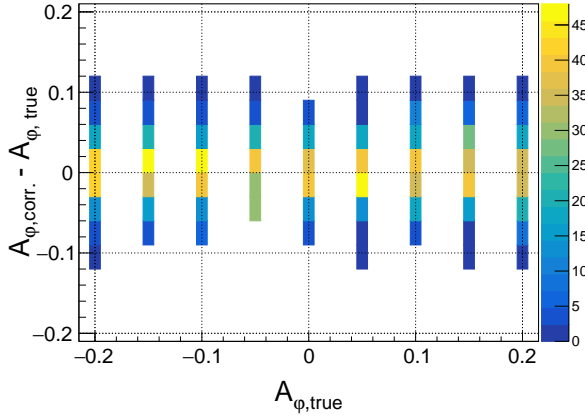


FIG. 6: Difference between the corrected reconstructed asymmetry and the true asymmetry in nine MC ensembles. The ensembles are generated with asymmetries ranging from -20 % to +20 % in steps of 5 % and each consists of 125 samples that match our data in size. The bin width along the y -direction is roughly equal to the root-mean-square deviation.

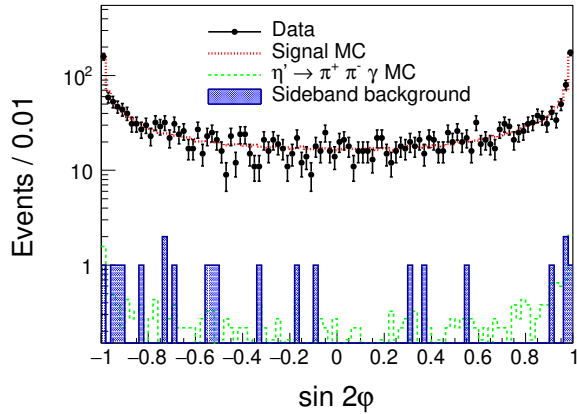


FIG. 7: Distribution of $\sin 2\phi$ after the photon conversion veto. Dots with error bars represent data, the dotted (red) histogram represents the signal MC sample generated with a symmetric $\sin 2\phi$ distribution, the dashed (green) histogram represents the remaining background contribution from $\eta' \rightarrow \pi^+ \pi^- \gamma$ events and the filled (blue) histogram the η' sideband contribution.

the kinematic fit and PID is found to be $\chi^2_{4C+PID} < 140$. After these initial selection criteria, the inclusive MC sample shows significant contamination from events with $\pi^0 \rightarrow \gamma\gamma$ or $\eta \rightarrow \gamma\gamma$. Such events can be separated from the signal by studying the energy distribution of the photon from the η' decay, and requiring $E_\gamma > 0.15$ GeV. The final signal yield is extracted by a fit to the $\pi^+ \pi^- \gamma$ -invariant mass distribution shown in Fig. 8. The signal is represented by the MC line shape convolved with a Gaussian function in order to take into account the difference in resolution between data and MC simulations. Continuous background is represented by a second order

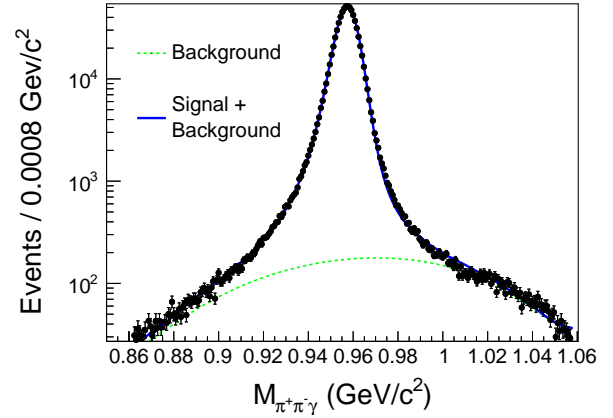


FIG. 8: Fit to the invariant mass distribution of $\pi^+ \pi^- \gamma$. Dots with error bars represent data, the dashed (green) line represents continuous background, and the solid (blue) line is the sum of the signal and background contributions.

Chebyshev polynomial. The yield and efficiency for the normalization channel are listed in Table I.

IV. SYSTEMATIC UNCERTAINTIES

A list of all sources of systematic uncertainties is given in Table III and details of how their contributions are estimated are given below:

- **MDC Tracking** The data-MC efficiency difference for pion track-finding has been studied using a control sample of $J/\psi \rightarrow p\bar{p}\pi^+\pi^-$ events. For the tracking of electrons, a mixed sample of $e^+e^- \rightarrow \gamma e^+e^-$ at the J/ψ meson mass and $J/\psi \rightarrow e^+e^- (\gamma_{FSR})$ was used. In both cases, the data-MC difference, $\Delta_{syst.}$, is extracted as a function of the particle momentum and the cosine of the polar angle. Subsequently, each event in the MC samples is re-weighted by a factor $(1 + \Delta_{syst.})$. The branching fraction and asymmetry parameter are recalculated with efficiencies determined from the re-weighted MC sample, and the difference from the original result is taken as the systematic uncertainty.
- **PID** The effect of the difference in PID efficiency between data and MC is evaluated in the same way as for the MDC tracking efficiency above. The control samples used are $J/\psi \rightarrow \pi^+\pi^-\pi^0$ for pions and $e^+e^- \rightarrow \gamma e^+e^-$ at the J/ψ meson mass and $J/\psi \rightarrow e^+e^- (\gamma_{FSR})$ for electrons.
- **Photon Reconstruction** The data-MC difference in the photon reconstruction efficiency has been studied based on a number of control samples, including $J/\psi \rightarrow \rho^0\pi^0$, $e^+e^- \rightarrow \gamma\gamma$ [31], and $e^+e^- \rightarrow \gamma\mu^+\mu^-$. It has been found that the average difference is 0.5% in the EMC barrel ($|\cos\theta_\gamma| < 0.80$),

and 1.5% in the endcaps ($0.86 \leq |\cos\theta_\gamma| \leq 0.92$). As for MDC tracking and PID, the MC samples are re-weighted event-by-event to correct these shifts.

- 4C Kinematic Fit** Using a control sample of $J/\psi \rightarrow \phi f_0(980)$, a set of correction factors for the track helix parameters is used within the BESIII collaboration to improve the agreement of the 4C kinematic fit performance between MC and data. The difference in branching fraction and asymmetry with and without these corrections is taken as the systematic uncertainty due to the kinematic fit.
- η' Mass Window** The effect of differences in the η' mass resolution between MC and data are evaluated by smearing the $\pi^+\pi^-e^+e^-$ and $\pi^+\pi^-\gamma$ invariant mass distributions according to the difference in resolution between data and MC as extracted from the fit in Fig. 8. The difference between the original result and the result with smearing is taken as the systematic uncertainty.
- Photon Conversion Veto** Systematic effects from the photon conversion veto are evaluated by introducing two alternative criteria for the invariant mass at beam pipe, and two for the opening angle Φ_{ee} , Fig. 4. The branching fraction and asymmetry parameters are calculated for all combinations of the original and alternative selection criteria. Half the largest difference from the original result is taken as the systematic uncertainty.
- Normalization** This is the combined systematic uncertainty for the normalization channel, including both the uncertainty on the known branching fraction $\mathcal{B}(\eta' \rightarrow \pi^+\pi^-\gamma)$ and uncertainties due to tracking, photon reconstruction, the requirement $E_{\gamma_{\eta'}} > 0.15$ GeV/c and effects from the range and background shape used in the fit to the $\pi^+\pi^-\gamma$ invariant mass distribution in Fig. 8. The photon energy cut, the fit range, and the background polynomial order are each varied and the largest changes caused by each are taken as systematic uncertainties. The value for $\mathcal{B}(\eta' \rightarrow \pi^+\pi^-\gamma)$ listed in the PDG is solely based on Ref. [32], using the same dataset. Thus, we take into account the strong correlation between the literature value of $\mathcal{B}(\eta' \rightarrow \pi^+\pi^-\gamma)$ and our analysis of the normalization channel. Due to small differences in the selection procedure, our final sample is a subset of the sample used in Ref. [32] with a correlation coefficient of 0.93 for the statistical uncertainty. For systematic uncertainties, we assume correlation coefficients to be one in case of sources that appear in both works, and zero for sources that appear only in one of the two works. The former case includes the systematic uncertainties regarding tracking, photon reconstruction, kinematic fitting, as well as range and background shape used in the

TABLE III: Systematic uncertainties on $\mathcal{B}(\eta' \rightarrow \pi^+\pi^-e^+e^-)$ and \mathcal{A}_φ . The systematic effects of MDC tracking, PID, and photon reconstruction on \mathcal{A}_φ are considered negligible compared to the other contributions.

Source	$\mathcal{B}(\eta' \rightarrow \pi^+\pi^-e^+e^-)$ [%]	$\mathcal{A}_\varphi (\times 10^{-2})$
MDC tracking	0.7	-
PID	3.0	-
Photon Reconstruction	0.6	-
4C Kinematic Fit	0.3	0.5
η' mass window	0.4	-
Photon Conversion Veto	0.8	0.9
Normalization	1.3	-
Total	3.5	1.1

fit. This systematic uncertainty only applies to the branching fraction.

V. RESULTS

Given the efficiencies and event yields in Table I, the ratio $\mathcal{B}(\eta' \rightarrow \pi^+\pi^-e^+e^-)/\mathcal{B}(\eta' \rightarrow \pi^+\pi^-\gamma)$ is determined to be $(8.20 \pm 0.16_{stat.} \pm 0.27_{syst.}) \times 10^{-3}$. Taking into account the world average of the branching fraction of $\eta' \rightarrow \pi^+\pi^-\gamma$ [24], the branching fraction of $\eta' \rightarrow \pi^+\pi^-e^+e^-$ is $(2.42 \pm 0.05_{stat.} \pm 0.08_{syst.}) \times 10^{-3}$. The statistical uncertainty has been improved by a factor of two compared to the last BESIII result, which is superseded by the result of this work due to the inclusion of the additional data collected in 2012. Ref. [2] predicts the branching fraction from two different VMD models (the hidden gauge model and the modified VMD model), to be $(2.17 \pm 0.21) \times 10^{-3}$ and $(2.27 \pm 0.13) \times 10^{-3}$ respectively. The unitary chiral perturbation theory approach of Ref. [3] yields a branching fraction of $(2.13^{+0.17}_{-0.31}) \times 10^{-3}$. Our result is consistent with all three predictions; it is about one standard deviation higher than each of them. The CP-violating asymmetry is determined to be $(2.9 \pm 3.7 \pm 1.1)\%$, which is consistent with zero. This work achieves precision comparable to that of the asymmetry measurement in the $K_L^0 \rightarrow \pi^+\pi^-e^+e^-$ decay [6, 7], but the size of the asymmetry determined here is significantly smaller than the SM driven effect of $(14 \pm 2)\%$ observed in the K_L^0 decay.

VI. ACKNOWLEDGEMENT

The BESIII collaboration thanks the staff of BEPCII and the IHEP computing center for their strong support. This work is supported in part by National Key Basic Research Program of China under Contract No. 2015CB856700; National Natural Science Foundation of China (NSFC) under Contracts Nos.

11625523, 11635010, 11735014, 11675184; National Natural Science Foundation of China (NSFC) under Contract No. 11835012; the Chinese Academy of Sciences (CAS) Large-Scale Scientific Facility Program; Joint Large-Scale Scientific Facility Funds of the NSFC and CAS under Contracts Nos. U1532257, U1532258, U1732263, U1832207; CAS Key Research Program of Frontier Sciences under Contracts Nos. QYZDJ-SSW-SLH003, QYZDJ-SSW-SLH040; 100 Talents Program of CAS; INPAC and Shanghai Key Laboratory for Particle Physics and Cosmology; German Research Foundation DFG under Contract No. Collaborative Research Center CRC 1044; Istituto Nazionale di Fisica Nucleare, Italy;

Koninklijke Nederlandse Akademie van Wetenschappen (KNAW) under Contract No. 530-4CDP03; Ministry of Development of Turkey under Contract No. DPT2006K-120470; National Science and Technology fund; The Knut and Alice Wallenberg Foundation (Sweden) under Contract No. 2016.0157; The Royal Society, UK under Contract No. DH160214; The Swedish Research Council; U. S. Department of Energy under Contracts Nos. DE-FG02-05ER41374, DE-SC-0010118, DE-SC-0012069; University of Groningen (RuG); The Helmholtzzentrum fuer Schwerionenforschung GmbH (GSI), Darmstadt and the Olle Engkvist Foundation (Sweden) under Contract No. 200-0605.

-
- [1] J. Sakurai, *Annals of Physics* **11**, 1 (1960).
 - [2] T. Petri, PhD thesis, Forschungszentrum Julich, (2010), arXiv:1010.2378[nucl-th].
 - [3] B. Borasoy and R. Nissler, *Eur. Phys. J. A* **33**, 95 (2007).
 - [4] M. Ablikim *et al.*, (BESIII Collaboration), *Phys. Rev. Lett.* **120**, 242003 (2018).
 - [5] E. Witten, *Nucl. Phys. B* **223**, 422 (1983).
 - [6] A. Alavi-Harati *et al.*, (KTeV Collaboration), *Phys. Rev. Lett.* **84**, 408 (2000).
 - [7] L. Iconomidou-Fayard, (NA48 Collaboration), *Int. J. Mod. Phys. A* **17**, 3012 (2002).
 - [8] C. Q. Geng, J. N. Ng, and T. H. Wu, *Mod. Phys. Lett. A* **17**, 1489 (2002).
 - [9] D.-N. Gao, *Mod. Phys. Lett. A* **17**, 1583 (2002).
 - [10] L. Gan, B. Kubis, E. Passemar, and S. Tulin, (2020), arXiv:2007.00664hep-ph.
 - [11] P. Naik *et al.*, (CLEO Collaboration), *Phys. Rev. Lett.* **102**, 061801 (2009).
 - [12] M. Ablikim *et al.*, (BESIII Collaboration), *Phys. Rev. D* **87**, 092011 (2013).
 - [13] P. Adlarson *et al.*, (WASA-at-COSY Collaboration), *Phys. Rev. C* **94**, 065206 (2016).
 - [14] F. Ambrosino *et al.*, (KLOE Collaboration), *Phys. Lett. B* **675**, 283 (2009).
 - [15] M. Ablikim *et al.*, (BESIII Collaboration), *Chin. Phys. C* **41**, 013001 (2017).
 - [16] M. Ablikim *et al.*, *Chin. Phys. C* **44**, 040001 (2020).
 - [17] M. Ablikim *et al.*, (BESIII Collaboration), *Nucl. Instrum. Meth. A* **614**, 345 (2010).
 - [18] C. Yu *et al.*, in *Proc. of International Particle Accelerator Conference (IPAC'16)*, Busan, Korea, May 8-13, 2016, pp. 1014–1018.
 - [19] S. Agostinelli *et al.*, (GEANT4), *Nucl. Instrum. Meth. A* **506**, 250 (2003).
 - [20] Z.-Y. Deng *et al.*, *Chin. Phys. C* **30**, 371 (2006).
 - [21] S. Jadach, B. F. L. Ward, and Z. Was, *Comput. Phys. Commun.* **130**, 260 (2000).
 - [22] R.-G. Ping, *Chin. Phys. C* **32**, 599 (2008).
 - [23] EvtGen Website: <https://phab.hepforge.org/source/evtgen/repository/master/>.
 - [24] P. A. Zyla *et al.*, (Particle Data Group), *Prog. Theor. Exp. Phys.* **2020**, 083C01 (2020).
 - [25] R.-L. Yang, R.-G. Ping, and H. Chen, *Chin. Phys. Lett.* **31**, 061301 (2014).
 - [26] E. Richter-Was, *Phys. Lett. B* **303**, 163 (1993).
 - [27] R.-G. Ping and C.-Y. Pang, Monte Carlo Generators for Tau-Charm-Physics at BESIII, http://bes.ihep.ac.cn/bes3/phy_book/book/phy/generators_ping.pdf.
 - [28] Z.-Y. Zhang, L.-Q. Qin, and S.-S. Fang, *Chin. Phys. C* **36**, 926 (2012).
 - [29] T. K. Pedlar *et al.*, (CLEO Collaboration), *Phys. Rev. D* **79**, 111101 (2009).
 - [30] A. Adare *et al.*, (PHENIX Collaboration), *Phys. Rev. C* **81**, 034911 (2010).
 - [31] M. Ablikim *et al.*, (BESIII Collaboration), *Phys. Rev. D* **81**, 052005 (2010).
 - [32] M. Ablikim *et al.*, (BESIII Collaboration), *Phys. Rev. Lett.* **122**, 142002 (2019).